PHYSICAL REVIEW B VOLUME 27, NUMBER 12 15 JUNE 1983

Solid-to-solid phase transition in crystalline benzil: A Raman scattering study

D. R. Moore*
Department of Physics, University of Illinois at Chicago, Chicago, Illinois 60680

V. J. Tekippe
Gould Research Center, Rolling Meadows, Illinois 60008

A. K. Ramdas
Department of Physics, Purdue University, West Lafayette, Indiana 47907

J. C. Toledano
Centre National d'Etudes des Télécommunications, F-92220 Bagneux, France
(Received 22 February 1983)

Benzil, which crystallizes at $T=368$ K in the trigonal space group $P3_121$ (D_3^4), undergoes a solid-to-solid phase transition at $T_c=84$ K with monoclinic $C2$ (C_2^3) symmetry below T_c; the primitive unit cell below T_c shows a fourfold expansion. Raman spectra associated with modes in which benzil molecules execute rigid translatory and rotatory (librational) oscillations—the external modes—show the consequences of the lowered symmetry and the unit-cell enlargement below T_c. The doubly degenerate zone-center E modes in the high-temperature phase show splittings, one of which manifests a pronounced softening and a discontinuity in its frequency at T_c characteristic of a first-order transition. The zone-boundary external modes associated with the M points of the Brillouin zone for $T>T_c$ transform into Raman-active zone-center phonons below T_c. The Raman spectra at $T\leq T_c$ show a large number of new lines which can be attributed to these zone-boundary M modes; one of these is a second soft mode related to the unit-cell enlargement. The experimental results are discussed in terms of a model in which the M-point instability is triggered by the one at the zone center.

I. INTRODUCTION

The organic compound benzil, $C_6H_5COCOC_6H_5$, crystallizes at 368 K with a space group D_3^4 ($P3_121$) or its enantiomorph D_3^6 ($P3_221$).[1] At the temperature $T_c=84$ K it undergoes a solid-to-solid phase transition to a low-temperature form having C_2^3 ($C2$) space-group symmetry.[2,3] This fascinating organic crystal has been aptly labeled[4] as "organic quartz," it being isomorphous with α quartz, Te, Se, etc. in the temperature range $368>T>84$ K. Raman,[4–8] Brillouin,[9,10] and infrared spectroscopy[11] have been applied to the study of the zone-center optical and acoustic phonons of this crystal. In the trigonal phase, benzil crystal consists of three molecules arranged in a spiral fashion along the threefold axis in a manner identical to the three Te atoms in crystalline Te. We note that the benzil molecule consists of two $C_6H_5-C=O$ units coupled by a carbon–carbon bond, such molecules in turn being bonded to others by weak van der Waals intermolecular forces. The earlier studies of Solin and Ramdas,[5] Claus *et al.*,[4] and Stenman[6] identified the Raman lines characteristic of the coupled intramolecular vibrations ("internal modes") and the coupled intermolecular vibrations and rotations ("external modes") in the trigonal phase. Sapriel *et al.*[7] and Moore *et al.*[8] addressed themselves specifically to the manifestations of the $T_c=84$ K solid-to-solid phase transition in the Raman spectrum. Vacher *et al.*[10] investigated this phase transition as it reveals itself in the Brillouin spectrum and hence in the elastic compliance constants.

It is clearly of interest to establish the nature of the solid-to-solid phase transition at $T_c=84$ K. Esherick and Kohler[2] made the striking observation that below the transition temperature uniaxial benzil becomes biaxial. On the basis of conoscopic interference figures they noted that the optic axial angle $2V$ between the optic axes observed in the low-temperature phase dropped from 24° to 0° at the transition temperature; below 84 K, $2V$ increased

linearly with decreasing temperature. Though the discontinuity in $2V$ as a function of temperature suggested a first-order transition, the complete reversibility of the onset or disappearance of the birefringence and a vanishingly small latent heat led them to believe that the phase transition might be second order in character. Dworkin and Fuchs[12] reported a very sharp peak at $T=84.07$ K in the heat capacity; the earlier failure to observe a measurable latent heat was attributed by these authors to a lack of adequate temperature resolution. They concluded that the 84-K phase transition is "nearer first order than second order."

Raman scattering has proved to be very fruitful in providing a microscopic insight into the nature of phase transitions.[13] With this motivation, the present authors have carried out a detailed study of the temperature dependence of the Raman-active low-frequency external modes in benzil. While the work reported in this paper[14,15] was in progress, Sapriel *et al.*[7] reported the temperature dependence of the lowest-frequency doubly degenerate E mode in the trigonal phase with a room-temperature position of 16 cm^{-1}; as the temperature was lowered this line "softened" nonlinearly and, below T_c, split into two lines. No discontinuity in frequency was apparent in their work. This behavior is consistent with a second-order phase transition from trigonal to monoclinic symmetry. Complementary optical measurements of the crystal below T_c revealed a multidomain structure having three domains differing from one another by a 120° rotation about the original threefold axis. Each domain contained an extinction direction coincident with one of the three twofold axes of the trigonal phase. These results are also consistent with a monoclinic symmetry. However, the x-ray diffraction studies of Odou *et al.*[3] were interpreted as indicating a triclinic symmetry below T_c. The observed soft mode—the 16-cm^{-1} E mode referred to above—is a zone-center mode which typically induces a phase transition preserving the number of atoms per unit cell.[16] On the other hand, the x-ray studies showed a fourfold increase in the unit cell whereas the Raman study of Sapriel *et al.*[7] showed no evidence of the enlargement of the unit cell. In a recent publication[17] one of us resolved some of the inconsistencies by reinterpreting the x-ray data and developed a phenomenological model for the phase transition at T_c. We have made a careful comprehensive study of the low-frequency Raman spectrum over a large temperature range including T_c. The purpose of this paper is to present our results which clearly show the consequences of the monoclinic symmetry and the unit-cell enlargement below T_c; we are able to interpret them in a self-consistent manner in the light of the phenomenological theory developed in Ref. 17.

II. THEORETICAL CONSIDERATIONS

As is well known, the first-order Raman spectrum of a crystal is restricted to long-wavelength optical excitations with wave vectors ($\vec{q}$) small compared to the dimensions of the Brillouin zone, i.e., to the zone-center optical phonons. The corresponding normal coordinates form the bases for the irreducible representations of the point-group symmetry of the crystal.[18,19] In this paper our focus is on the external vibrations of the benzil molecules since we expect the phase transition at T_c to affect them in an especially marked manner. In the external vibrations the benzil molecules vibrate as units—either in "rigid" translations against one another or in rotatory (librational) motions about the bonds between them.

A. $T > T_c$

At temperatures above T_c and below its melting point, the point-group symmetry of benzil is D_3 and the zone-center external optical modes are distributed among the irreducible representations as $2A_1+3A_2+5E$ (Ref. 5); A_1, A_2, and E are the totally symmetric, the antisymmetric, and the doubly degenerate irreducible representations of D_3, respectively.[20] The optical modes belonging to A_1 are Raman active and infrared inactive; A_2 modes are Raman inactive and infrared active, and E modes are active in both (Table I). As a result of the long-

TABLE I. Zone-center external optical modes in benzil.

Point group	Mode symmetry	Translatory	Rotatory	Raman	Infrared
D_3 ($T > T_c$)	A_1	1	1	active	inactive
	A_2	1	2	inactive	active
	E	2	3	active	active
C_2 ($T < T_c$)	A	16	17	active	active
	B	17	19	active	active

range polarization field associated with them, the frequencies of the A_2 modes may show a variation from ω(LO) to ω(TO) as $\vec{q}$ changes in direction from parallel to the optic axis (c) to perpendicular to it. For a similar reason, E modes could split into ω(LO) and ω(TO) for $\vec{q} \perp c$ whereas only ω(TO) corresponds to $\vec{q} \| c$.

B. $T < T_c$

A reinterpretation[17] of the x-ray data of Odou *et al.*[3] has shown that benzil has the monoclinic space group C_2^3 below T_c preserving one of the three C_2 axes present above T_c. In addition, the two primitive translations in the basal plane of the high-temperature phase doubled below T_c in turn resulting in a fourfold expansion of the primitive unit cell. Figure 1 shows the relative orientation of the lattice vectors in the two phases. We note that as a result of the fourfold expansion of the unit cell at the phase transition, the primitive unit cell contains 12 benzil molecules. Thus a total of $36-3$ translatory and 36 rotatory zone-center external vibrations are expected below T_c.

Since only two of the 12 molecules in the unit cell of benzil for $T < T_c$ retain the C_2-site symmetry it can be shown that there will be $16A+17B$ translatory and $17A+19B$ rotatory external vibrations (Table I). Of these, $3A+3B$ translatory and $4A+5B$ rotatory modes have their origin in the zone-center external modes of the high-temperature D_3 phase; here we have used $A_1 \rightarrow A$, $A_2 \rightarrow B$, and $E \rightarrow A+B$, the correlations between the irreducible representations of the high-temperature D_3 and the low-temperature C_2 phases, respectively (Table II). The remaining $13A+14B$ translatory and $13A+14B$ rotatory modes in the C_2 phase must be attributed to the fourfold expansion of the unit cell during the phase transition. In the high-temperature D_3 phase, these additional modes correspond to the zone-boundary phonons with $\vec{q}$ vectors equal to the k vectors of the M points of the hexagonal Brillouin zone of the trigonal lattice. Figure 2 shows the reciprocal-lattice vectors $\vec{g}_1$ and $\vec{g}_2$ associated with the lattice vectors $\vec{a}_1$ and $\vec{a}_2$ in the basal plane of the trigonal lattice. The three distinct M points located at $\frac{1}{2}\vec{g}_1$, $\frac{1}{2}\vec{g}_2$, and $\frac{1}{2}(-\vec{g}_1+\vec{g}_2)$ form the three arms of the star of the M point, $\vec{k}^*_M$. The doubling of the translational periodicity along $\vec{a}_1$ and $\vec{a}_2$ observed by Odou *et al.*[3] results in the halving of the Brillouin zone in the basal plane. The M points, initially on the boundary of the Brillouin zone for $T > T_c$, are folded back to the center of the Brillouin zone for $T < T_c$; thus the zone-boundary phonons corre-

TABLE II. Correlation between phonon symmetry in the high-temperature (D_3) and the low-temperature (C_2) phases of benzil.

D_3	C_2
$2A_1+3A_2+5E$ $(q \sim 0)$	$7A+8B$ $(q=0)$
$8\Gamma_1(\vec{k}^*_M)+10\Gamma_2(\vec{k}^*_M)$	$26A+28B$ $(q=0)$
A_1	A
A_2	B
E	$A+B$
$\Gamma_1(\vec{k}^*_M)$	$2A+B$
$\Gamma_2(\vec{k}^*_M)$	$A+2B$

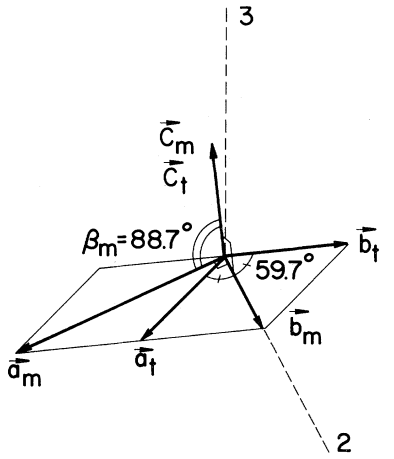

FIG. 1. Relative orientation of the lattice vectors of the triclinic ($\vec{a}_t, \vec{b}_t, \vec{c}_t$) and monoclinic ($\vec{a}_m, \vec{b}_m, \vec{c}_m$) unit cell of the low-temperature phase of benzil (See Ref. 17). Angles shown correspond to those at $T=80$ K. Note that the direction $\vec{c}_m$ is perpendicular to $\vec{b}_m$. Also shown are the threefold and a twofold axis of the trigonal phase.

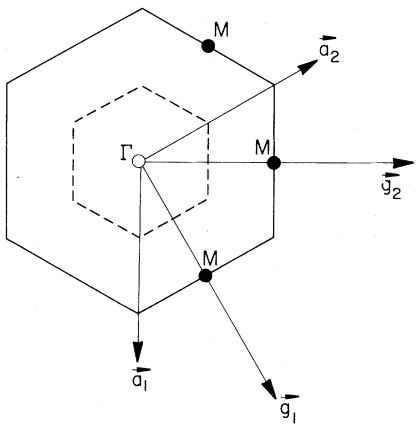

FIG. 2. First Brillouin zone (solid line) of the trigonal phase of benzil. Dotted line illustrates the folding of this zone as a result of a doubling of the lattice parameters along $\vec{a}_1$ and $\vec{a}_2$. Note that this zone folding causes the M points to coincide with the center of the Brillouin zone (Γ point).

sponding to $\vec{k}_M$ become zone-center phonons and manifest themselves in the first-order Raman spectrum, modes belonging to both A and B symmetry of C_2 being Raman active.

The symmetry properties of the normal modes of benzil belonging to the star of M are determined by the irreducible representation of the space group D_3^4 ($P3_121$). One can show that the zone-boundary phonons belonging to $\vec{k}_M^*$ are distributed among the two three-dimensional irreducible representations of the M point,[21] $\Gamma_1(\vec{k}_M^*)$ and $\Gamma_2(\vec{k}_M^*)$, as $8\Gamma_1(\vec{k}_M^*)+10\Gamma_2(\vec{k}_M^*)$. Further, in the C_2 phase, they become zone-center phonons according to the correlations $\Gamma_1(\vec{k}_M^*)\rightarrow 2A+B$ and $\Gamma_2(\vec{k}_M^*)\rightarrow A+2B$.[22] Thus, below T_c, we have $26A+28B$ zone-center optical phonons originating from the M points of the Brillouin zone of the high-temperature phase (Table II). These correspond precisely to the sum of the $13A+14B$ translatory and $13A+14B$ rotatory modes already deduced above. Figure 3 gives a pictorial representation of the relationship between the modes in the D_3 and C_2 phases consistent with the unit-cell enlargement in the C_2 phase. The polarizability tensors of the Raman-active modes are also shown in the diagram.

C. Phase-transition theory

According to the Landau theory of continuous phase transitions,[23] the high-symmetry phase becomes unstable at the transition temperature T_c with respect to the so-called order parameter η. The order parameter transforms according to an irreducible representation $\Gamma(\vec{k}^*)$ of the space group of the high-symmetry phase, where $\vec{k}^*$ is a star of $\vec{k}$ vectors in the first Brillouin zone.[24] The change in translational symmetry which occurs at the transition is directly related to $\vec{k}^*$.[25] Owing to the gradual nature of the phase transition and the small value of η near T_c, the free energy of the system can be expanded in a power series in η. When the order parameter corresponds to the eigenvector of a normal mode of the crystal lattice, the frequency of this normal mode tends to zero (i.e., softens) as T approaches T_c from above and below.[13,16] This corresponds to a "freezing in" of the normal-mode displacements in the structure of the high-symmetry phase. Hence the structure of the low-temperature phase is determined by the superposition of the structure of the high-temperature phase and the eigenvector of the "soft" mode.[26] Therefore, the symmetry change and the soft mode are related to the same irreducible representation $\Gamma(\vec{k}^*)$. Although the Landau theory assumes a continuous second-order phase transition, it can also be applied to weakly first-order transitions.[16]

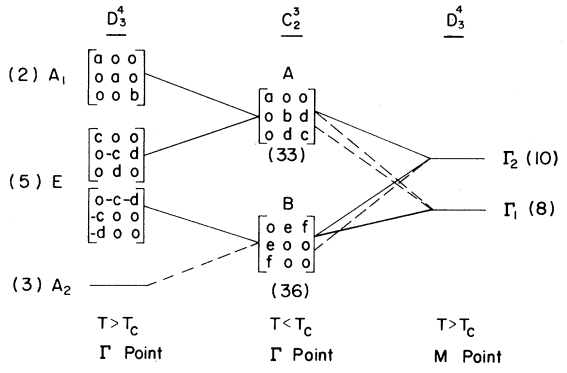

FIG. 3. Group-theoretical analysis of the phase transition in benzil. Lines indicate the correlation of the modes in the trigonal phase above T_c with those of the monoclinic phase below T_c. Solid lines indicate those modes which are expected to show strong Raman activity. Also shown are the polarizability tensors of the Raman-active modes.

The case of benzil is somewhat complicated for it to be handled by the simple Landau theory, however; an optic mode of E symmetry, related to $q=0$, is observed to soften in the trigonal phase, while the change in the translational symmetry resulting in the fourfold expansion of the unit cell corresponds to an instability at $\vec{k}_M^*$. Thus the changes in the crystal that occur at the transition are not related to the same star of $\vec{k}$ vectors and a different type of mechanism needs to be investigated. Holakovsky[27] has suggested that an instability with respect to one order parameter $\{\zeta_i\}$ can be triggered by an instability with respect to another order parameter $\{\eta_i\}$. In general, $\{\eta_i\}$ and $\{\zeta_i\}$ can have different symmetry characteristics. The phenomenological model in Ref. 17 explored this idea for the mechanism of the phase transition in benzil. The primary order parameter η is related to the atomic displacements of the soft optic E mode and has two components $\{\eta_x,\eta_y\}$. The secondary order parameter ζ, associated with the three-armed star of the M point of the hexagonal Brillouin zone, has three components $\{\zeta_1,\zeta_2,\zeta_3\}$ and belongs to the irreducible representation $\Gamma_2(\vec{k}_M^*)$. Symmetry considerations as applied to the model yield a coupling of the form $-\delta(\eta\zeta^2)$ between the two order parameters, where δ is the coupling constant. For a first-order phase transition, the instability relative to η is also first order. Further, if the above coupling is sufficiently strong, the instability with respect to η will in turn trigger an instability with respect to ζ and at T_c result in the onset of the spontaneous values η_S and ζ_S for η and ζ, respectively. In this manner the $E(q=0)$ soft mode inducing the phase transition can trigger an additional $\Gamma_2(k_M^*)$ soft mode.

As shown in Fig. 3, the soft E mode is expected to split into one A mode and one B mode at the phase

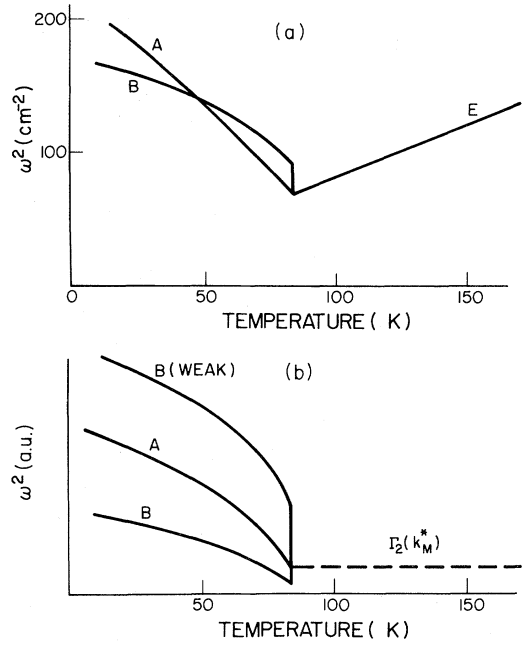

FIG. 4. Predicted temperature dependence of the squared frequencies of the soft modes of benzil: (a) the soft optic E mode associated with the symmetry change, and (b) the soft Γ_2 mode related to the enlargement of the unit cell (See Ref. 17).

transition. Similarly, the triggered soft Γ_2 mode will split into one A mode and two B modes. The temperature dependence of the square of the frequencies associated with these two soft modes has been predicted by the phenomenological model[17] and is shown in Fig. 4. Above T_c the square of the frequency of the soft E mode varies linearly with temperature and extrapolates to zero frequency at $T=0$ K. At T_c, the frequency of the B component is expected to jump discontinuously whereas that of the A component is continuous. In addition, the two modes are predicted to cross at ~ 50 K. As mentioned previously, the soft Γ_2 mode is Raman inactive in the upper phase. However, at T_c, its two B components undergo discontinuous changes, as in the case of the soft E mode. Below T_c, all three components arising from the Γ_2 mode are expected to be strongly temperature dependent, with the squared frequencies being proportional to the square of the spontaneous value of the triggered parameter ξ_s^2.

As shown earlier in this section, the monoclinic phase of benzil has potentially 69 Raman-active zone-center external modes. As can be seen in Fig. 3, 12 of them, $7A+5B$, are related to the Raman-active A_1 and E modes of the trigonal phase. The remaining 57 modes are associated with the Raman-inactive A_2 ($q=0$), Γ_1 ($\vec{k}_M^*$), and Γ_2 ($\vec{k}_M^*$) modes. As shown in the Appendix, these modes can acquire Raman activity at the phase transition via an activation process involving an anharmonic coupling to the Raman-active modes.

The relative strengths of the various lattice modes which become Raman active below T_c can be deduced on the basis of the Raman activity determined by the lowest-order coupling terms allowed by symmetry. In the case of benzil, we have considered the coupling of the previously Raman-inactive A_2, Γ_1, and Γ_2 modes with the Raman-active A_1- or E-symmetry modes. The forms of the lowest-order coupling terms are displayed in Table III. The Raman activity of an A_2 mode, for example, can only occur via a coupling to an E mode. To lowest order, this coupling is of degree 4 and is likely to be weak. The Γ_1 modes, on the other hand, become Raman active by coupling to either A_1 or E modes. The lowest-order coupling with the E modes is of order 3 whereas that with the A_1 modes is of order 4. The Raman activity of the Γ_2 modes also is derived from their coupling to A_1 or E modes, the lowest-order

TABLE III. Lowest-order coupling between the Raman-inactive and the Raman-active modes of benzil.

Inactive mode and component	Active mode and component	Activating coupling term	Degree of coupling	Symmetry of activated mode below T_c
$A_2:\eta_2$	$A_1:\eta_1$			
$A_2:\eta_2$	$E:\{\eta_x,\eta_y\}$	$\eta_2\eta_y(3\eta_x^2-\eta_y^2)$	4	B
$\Gamma_1:\{\xi_1,\xi_2,\xi_3\}$	$A_1:\eta_1$	$\eta_1(\xi_1\xi_2\xi_3+\xi_2\xi_1\xi_3+\xi_3\xi_1\xi_2)$	4	A
	$E:\{\eta_x,\eta_y\}$	$\sqrt{3}(\xi_2\xi_2-\xi_3\xi_3)\eta_x$ $+(2\xi_1\xi_1-\xi_2\xi_2-\xi_3\xi_3)\eta_y$	3	B
$\Gamma_2:\{\xi_1,\xi_2,\xi_3\}$	$A_1:\eta_1$	$\eta_1(\xi_1^2+\xi_2^2+\xi_3^2)$	3	A
	$E:\{\eta_x,\eta_y\}$	$\eta_x(2\xi_1^2-\xi_2^2-\xi_3^2)$ $+\eta_y(\xi_2^2-\xi_3^2)$	3	B

coupling being 3 in either case. From the details of the coupling scheme shown in Table III, below T_c we expect to see one A and one B component for each Γ_1 and Γ_2 mode. The second A (B) component of the Γ_1 (Γ_2) mode has higher-order coupling terms and hence, in comparison, is expected to be weaker.

By using the coupling terms given in Table III and the group-theoretical results given in Fig. 3, the number and symmetry of the Raman-active modes of benzil expected as the temperature is lowered below T_c can be deduced; they are shown in Table IV. Above the transition temperature there are seven Raman-active modes ($2A_1$ and $5E$). Below T_c as many as 69 Raman-active modes are expected. However, some of these modes are only weakly coupled to the modes which are Raman active above T_c and hence are not likely to be observed. Owing to the vanishingly small latent heat[2] and the small spontaneous value of the order parameter η at T_c,[3,17] little change in the Raman spectra is expected at the phase-transition temperature, with two exceptions: (1) the anomalous behavior and splitting of the soft E mode of the trigonal phase, and (2) the appeareance of one A-symmetry and one B-symmetry component of the triggered soft Γ_2 mode. Thus just below the transition temperature only eight modes of A symmetry and six modes of B symmetry are expected to appear in the Raman spectrum. Note that the splitting of the E modes is expected to be weak at this temperature. As the temperature decreases, the splitting of the E modes will increase and the modes corresponding to the coupling terms of degree 3 will become observable. As a result, one additional A and B component for each of the remaining nine Γ_2 modes as well as the B component of the eight Γ_1 modes will appear in the Raman spectrum. Thus the Raman spectrum for $T < T_c$ can exhibit as many as 17 A and 23 B lines (see Table IV). At still lower temperatures, modes associated with fourth-order coupling terms involving the B components of A_2 modes and one A component of each of the Γ_1 modes may become observable. In principle, for $T \ll T_c$, the modes corresponding to the higher-order coupling terms (degree ≥ 5) can become observable giving a total of 33 A modes and 36 B modes. However, these modes are expected to remain weak, even at liquid-helium temperatures, and hence will probably not be observed.

III. EXPERIMENTAL PROCEDURE

The Raman spectrometer consisted of an Ar^+ laser and a scanning double monochromator; a thermoelectrically cooled photomultiplier together with a phase-sensitive detection system constituted the detection system. The details are given in Ref. 22. All the Raman spectra were excited with the 5145-Å line of Ar^+ passed through a narrow-band filter of ~ 12-Å bandwidth to eliminate any nonlasing plasma lines. The spectra were recorded with a typical incident power level of ~ 25 mW. A broad-band polarization rotator was used to set the plane of polarization of the linearly polarized laser radiation and a polaroid was employed to analyze the scattered radiation. A variable-temperature stainless-steel cryostat[28] together with a temperature controller[29] allowed measurements over the temperature range 2—300 K.

The benzil crystals were grown by the Bridgman method. The optic axis (Z) and the diad axis (X) were identified with x rays; here X, Y, and Z form a right-handed coordinate system and refer to the room-temperature phase of D_3 symmetry. The optic axis was also determined by locating the direction of zero birefringence; an examination of a specimen between a pair of polaroids with collimated white light showed a succession of bright colors as the analyzer is rotated. From such observations, the "handed-

TABLE IV. Temperature dependence of the Raman activity of the external modes of benzil.

Phonon-mode symmetry	$T > T_c$ (D_3^4)	$T \leq T_c$ ($\tilde{C}_2^3$)		$T < T_c$ (C_2^3) (degree 3)		$T < T_c$ (C_2^3) (degree 4)		$T \ll T_c$ (C_2^3) (degree > 5)	
		A	B	A	B	A	B	A	B
A_1	2	2		2		2		2	
A_2							3		3
E	5	5	5	5	5	5	5	5	5
Γ_1					8	8	8	16	8
Γ_2		1	1	10	10	10	10	10	20
Total	7	8	6	17	23	25	26	33	36

ness" of a specimen could be determined.[30] We found that the crystals used in this study are left handed and are free from fractures, twinning, domains, or inclusions. Samples from a boule were cut with the desired orientation using a wire saw and polished on lens paper dampened with xylene. Benzil crystals are susceptible to thermal shocks and care has to be exercised during sample preparation. Typical sample dimensions are $1\times1\times0.5$ cm^3.

From the polarizability tensors of the Raman-active modes shown in Fig. 3 it can be seen that the $Y(ZZ)X$ scattering geometry[31] isolates the A_1 modes in the trigonal and the A modes in the monoclinic phase. The Raman spectrum in the $Y(XY+XZ)X$ geometry, on the other hand, allows the identification of the E modes above T_c and the B modes below T_c. In practice, one has to contend with the birefringence and the optical activity in order to obtain unambiguous polarization results. In the trigonal phase one can avoid these disturbing factors by restricting the incident and the scattered directions to the plane normal to the optic axis (Z); the above scattering geometries were selected on this basis. However, in the monoclinic-biaxial phase only the X axis of the trigonal phase remains as a principal axis of the triaxial ellipsoid representing the indicatrix. Thus in the above right-angle scattering geometries, either the incident or the scattered polarization could allow the A modes to appear in the $Y(XY+XZ)X$ geometry and the B modes in the $Y(ZZ)X$ geometry; the presence of domains in the monoclinic phase can introduce additional complications in the polarization studies. These effects were minimized by observing the scattered radiation along X while confining the incident radiation to Y. Experimentally, the "leakages" of the forbidden line in the scattering geometries were found to be minimal.

IV. EXPERIMENTAL RESULTS AND DISCUSSION

Figure 5 shows the room-temperature Raman spectrum of benzil spanning both the internal and external modes. By far, the larger number of lines occur in the range 100—3300 cm^{-1} and they can be attributed to the internal modes.[5,6] The external modes[4,7,22] have shifts less than 100 cm^{-1} and are shown to the left of the vertical dashed line at 100 cm^{-1}; note that the intensity scale for the external modes is $\sim$30 times larger than that for the internal modes. In the remainder of this section our focus is on the external modes.

Figure 6 shows the room-temperature Raman spectrum of benzil in the (0—100)-cm^{-1} range recorded in the $X(YX+YZ)Y$ and the $X(ZZ)Y$ polarization configurations. The stray-light rejection of the spectrometer and the good optical quality of

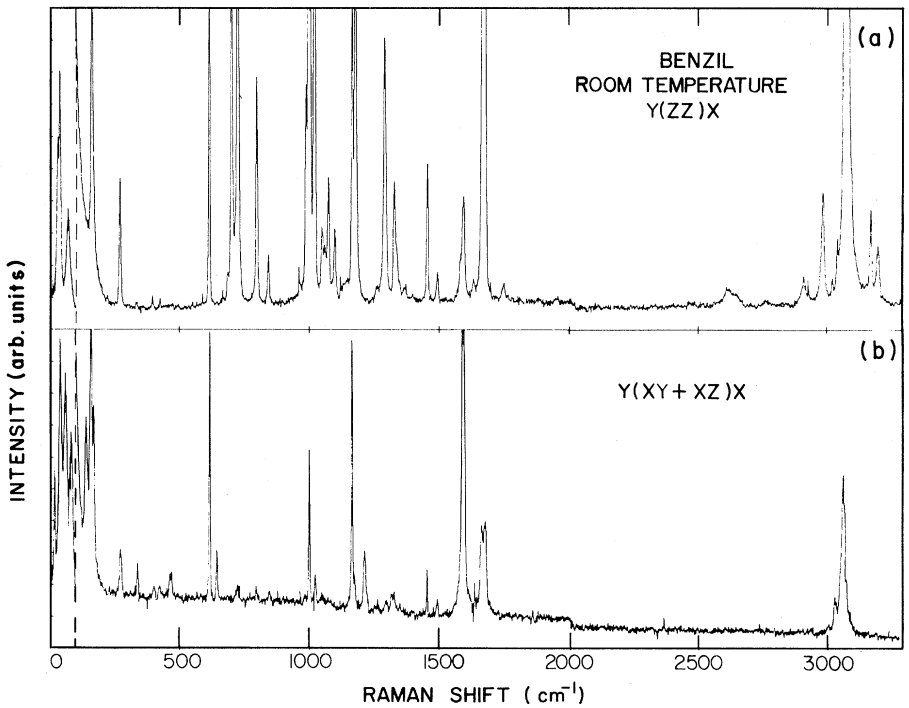

FIG. 5. Room-temperature Raman spectra of benzil showing both the internal and external modes of (a) A_1 symmetry and (b) E symmetry.

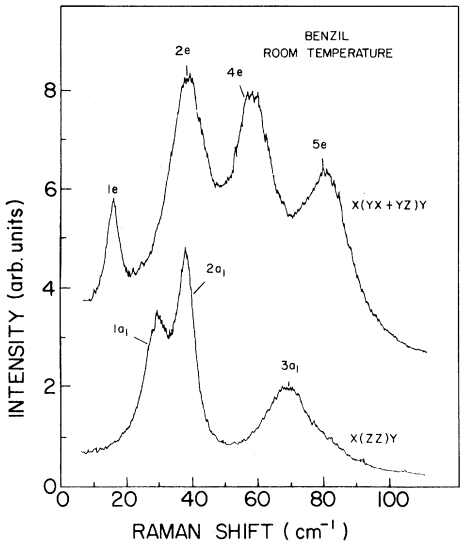

FIG. 6. Room-temperature Raman spectra of benzil showing the external modes of E symmetry (upper trace) and A_1 symmetry (lower trace). Upper trace has been shifted upwards for clarity.

the crystals enabled observation of Raman lines with shifts as small as 3 cm^{-1}. The spectra were recorded with a spectral slit width of ~ 1.5 cm^{-1}. Thus the halfwidths of the Raman lines are very close to their natural halfwidths. The Raman lines are labeled in the order of increasing frequency, with the line number followed by a lower-case letter designating its symmetry. For example, 4*e* identifies the fourth mode of E symmetry. The line assignments of the modes in the trigonal phase are based on the Raman spectra recorded just above T_c whereas the spectra recorded at $T = 16$ K were used to identify the modes in the monoclinic phase. The positions of the external modes for $T > T_c$ are listed in Table V; they are in good agreement with those reported by Claus *et al.*[4] and Sapriel *et al.*[7] The backscattering geometry employed by Sapriel *et al.* revealed a very small LO-TO splitting of the E modes. We also note that a variety of scattering geometries has been used in the three sets of data in Table V and there is very little evidence of frequency variation traceable to crystal anisotropy. All of the studies contain three instead of two A_1 lines predicted by group theory for $T > T_c$. Claus *et al.*[4] attribute the extra A_1 line at 29.1 cm^{-1} to a difference mode.

We now consider the effects of lowering the temperature to and below T_c. We recall at $T = T_c$ the crystal symmetry changes from D_3 to C_2 and the volume of the primitive cell increases by a factor of 4. In Fig. 7 we show the $Y(XY+XZ)X$ spectrum in which the E modes for $T \geq T_c$ and the B modes for $T < T_c$ are allowed. As the temperature approaches T_c from above, the intensity of the lowest E mode having a frequency of 15.8 cm^{-1} at room temperature increases dramatically; its frequency, on the other hand, decreases. This striking behavior is characteristic of a soft mode which induces a phase transition. Consistent with the arguments concerning intensities presented in Sec. II, we do not observe any drastic changes in the Raman spectrum close to T_c except for the emergence of a new line (2*b*) on

TABLE V. Frequencies of Raman-active external phonons at room temperature in cm^{-1}.

Line	Symmetry species		Present study[a]	Raman shifts (cm^{-1}) Sapriel *et al.*[b]	Claus *et al.*[c]
1*e*	E	TO	15.8	15.1	16
		LO		15.3	
$1a_1$	A_1		29.1	28.8	30
$2a_1$	A_1		37.6	37.6	39
2*e*	E	TO	38.0	37.9	39
		LO		38.8	
3*e*[d]	E	TO			
		LO			
4*e*	E	TO	58.1	57.0	58
		LO		57.8	
$3a_1$	A_1		69.7	68.8	69
5*e*	E	TO	80.8	82.5	78
		LO		82.5	

[a] A_1 modes: $X(ZZ)Y$, $Y(ZZ)X$; E modes: $X(YX+YZ)Y, Y(XY+XZ)X$.
[b] A_1 modes: $Y(XX)\bar{Y}, Y(ZZ)\bar{Y}, X(YY)\bar{X}, X(ZZ)\bar{X}$; E(TO) modes: $Y(XX)\bar{Y}$; E(LO) modes: $Y(XZ)\bar{Y}, X(YY)\bar{X}, X(YZ)\bar{X}$.
[c] A_1 modes: $X(ZZ)Y$; E modes: $X(YX)Y, X(ZX)Y$.
[d] Line 3*e*, at ~ 50 cm^{-1}, is seen only below 150 K.

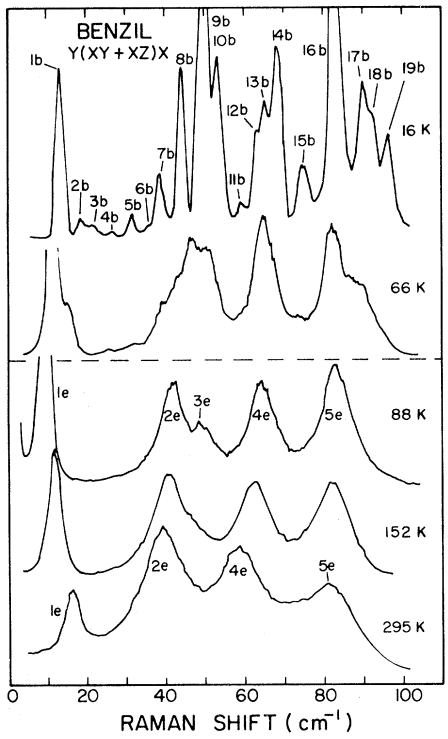

FIG. 7. Raman spectra exhibited by benzil at selected temperatures above and below T_c (dashed line). Scattering geometry used allows E modes above T_c and B modes below T_c.

the shoulder of the B component of the soft E mode ($1b$). We interpret this new line as the stronger B component of the soft Γ_2 mode. On lowering the temperature further, additional Raman lines manifest themselves and at 16 K a total of 19 Raman-active B modes are observed. This is in good agreement with the 23 B modes expected in the polarized Raman spectra exhibiting modes activated by coupling terms up to degree 3, and provides an excellent confirmation of the cell multiplication associated with the phase change. The two soft-mode components $1b$ and $2b$ are clearly singled out by the temperature dependence of their frequencies; as the temperature decreases they become less intense and shift to higher frequencies. This contrasts with the general increase in intensity exhibited by the other external modes.

The Raman spectra showing the A_1 and A lines are shown in Fig. 8 where the scattering geometry $Y(ZZ)X$ allows them to appear. The intensity of line $1a_1$ at 29.1 cm^{-1} decreases with decreasing temperature already in the trigonal phase; it is on the basis of this behavior that Claus *et al.*[4] attributed it to a difference mode. The other two A_1 modes at 37.6 cm^{-1} ($2a_1$) and 69.7 cm^{-1} ($3a_1$) increase in intensity with decreasing temperature. As can be seen in the figure, a small amount of $1e$ and $5e$ appears as leakage in the spectra recorded above 84 K. Since they are present in the spectra well above 84 K, their appearance is not related to the phase transition. As expected, no significant changes in the spectra are observed as the crystal undergoes the phase transition except for the increase in the intensity of the lowest-frequency mode labeled $1a$. This feature clearly cannot be attributed to leakage of the B component of the soft E mode since, as pointed out earlier, the intensity of the B component continually decreases upon cooling below T_c. On the other hand, line $1a$ steadily increases in intensity as the temperature decreases; we interpret it as the A component of the soft E mode. The intensity of the A component of the soft Γ_2 mode is expected to be weak at T_c and gradually strengthen as the temperature decreases. As seen in Fig. 8, the line labeled $3a$ exhibits this behavior and is identified as the A component of the soft Γ_2 mode. A detailed discussion of the temperature dependence of the components of the soft modes will be given presently. By 46 K more lines begin to emerge in the spectra and at 16 K a total of 17 Raman-active A modes are observed. This result also agrees very well with the number of

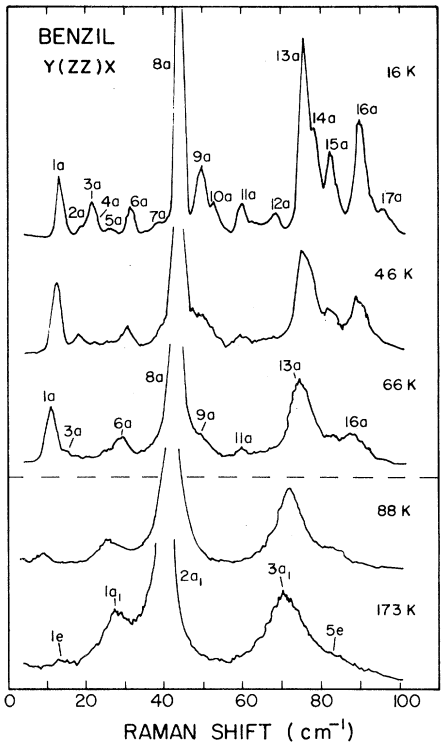

FIG. 8. Raman spectra exhibited by benzil at selected temperatures above and below T_c (dashed line). Scattering geometry used allows A_1 modes above T_c and A modes below T_c.

A modes in the Raman spectra originating from coupling terms of degree 3 as shown in Table III. The line labeled $8a$ is thought to actually consist of two accidentally degenerate A modes; a full discussion of this point will be given later.

The frequencies of the Raman-active external modes observed in the present study are plotted as a function of temperature in Figs. 9 and 10. The nonlinear behavior of the A and B components of the two soft modes is quite noticeable. Several other modes, located at higher frequencies, also exhibit significant nonlinear behavior near T_c; for example, line $16a$ moves from 83.4 at T_c to 90.1 cm^{-1} at 16 K. Three additional A-symmetry modes, $5a$, $6a$, and $13a$, as well as one B-symmetry mode, $9b$, also show similar behavior below T_c. It appears that these modes, like the soft modes, have atomic motions with eigenvectors which are related to the structural change.

As pointed out earlier, the identification of the soft modes is facilitated by their anomalous behavior near the phase transition. The frequencies of the soft modes measured in the present study are plotted as a function of temperature in Fig. 11. The frequency of the soft E mode of the trigonal phase decreases markedly from 15.8 cm^{-1} at room temperature to ~ 8 cm^{-1} at 84 K. The square of the frequency has a linear behavior in this temperature range. These results agree very well with the observations of Sapriel *et al.*[7] Below $T_c = 84$ K, the components of the soft modes exhibit a pronounced nonlinear temperature behavior. The A and B components (lines $1a$ and $1b$) of the soft E mode are nearly degenerate throughout most of the low-

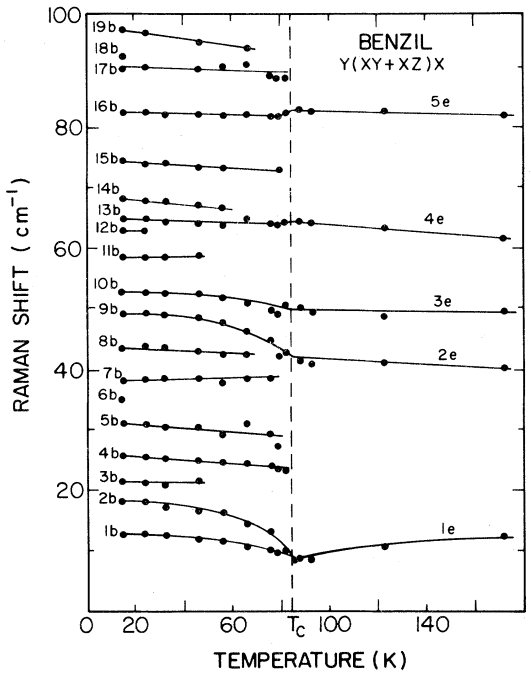

FIG. 9. Temperature dependence of the Raman shifts of the external modes of benzil above and below T_c (dashed line). Scattering geometry used allows E modes above T_c and B modes below T_c.

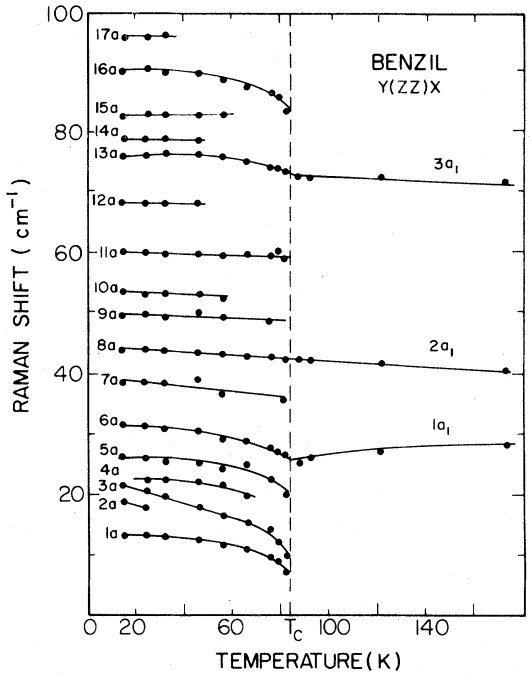

FIG. 10. Temperature dependence of the Raman shifts of the external modes of benzil above and below T_c (dashed line). The scattering geometry used allows A_1 modes above T_c and A modes below T_c.

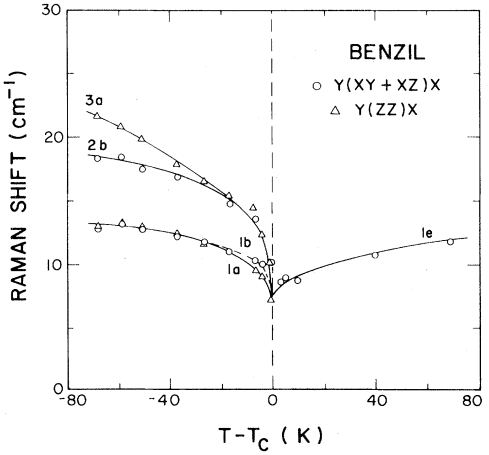

FIG. 11. Temperature dependence of the Raman shifts of the soft modes of benzil above and below T_c (dashed line). For the scattering geometries used, o indicates E modes above T_c and B modes below T_c. A modes below T_c are denoted by △.

temperature region and harden from ~ 8 to ~ 13 cm^{-1} upon cooling to 16 K. These data also show a possible discontinuity of ~ 1 cm^{-1} in the frequency of the B component ($1b$) and a merging of the frequencies of the A and B components at 56 K. Although these effects were predicted in Ref. 17, the resolution in this particular measurement does not allow a more definitive analysis; study of the discontinuity is given later. The frequencies of the A and B components (lines $3a$ and $2b$) of the soft Γ_2 mode exhibit a stronger temperature dependence than those of the soft E mode. At 16 K, the frequencies of the A and B components are 21.3 and 18.6 cm^{-1}, respectively. As the temperature approaches T_c from below, the two modes merge at ~ 66 K and soften considerably to ~ 8 cm^{-1} at T_c. The larger frequency change exhibited by the A component is consistent with the predictions of the model proposed in Ref. 17. As expected from the intensity considerations given earlier, the second B component of the soft Γ_2 mode was not observed.

Estimates of the integrated intensities of the soft modes are plotted as a function of temperature in Fig. 12. As noted previously in Fig. 7, the intensity of the soft E mode increases dramatically as the transition temperature is approached from above. Below T_c, the intensity of the B component (line $1b$) of the soft E mode is also quite large but quickly decreases upon further cooling. Similar behavior is observed for the corresponding A component (line $1a$) below T_c, but the effects of the $Y(ZZ)X$ scattering geometry force the intensity towards zero upon approaching T_c from below. Note that, due to the small leakage of the E mode in these measurements, the intensity of the A component does not appear to go to zero at T_c. Quite similar behavior, although not as pronounced, is also exhibited by the A and B components of the soft Γ_2 mode. The smaller intensities observed for these components are consistent with the triggering mechanism assumed in Ref. 17.

As discussed previously, the results in Fig. 11 suggest a small discontinuity in the frequency shift of the B component ($1b$) of the soft E mode at the phase transition. A detailed study was made of the very intense soft E mode above T_c to verify this result. The temperature of the sample was accurately monitored by embedding a calibrated thermocouple directly in the crystal. The measured frequency shift as a function of temperature is shown in Fig. 13. A discontinuous change in the Raman shift on the order of 1 cm^{-1} was observed over a very narrow temperature range around T_c. Although the crystal orientation used in these detailed measurements and its biaxial nature below T_c did not allow us to fully isolate the A and B components of the soft E modes, we are confident that the line exhibiting the discontinuity in Fig. 13 has predominantly B symmetry. It is interesting to note that *small hysteresis* effects were also observed as the temperature was cycled back and forth through T_c. Both of these observations are consistent with the (weakly) first-order nature of the phase transition and the predictions in Ref. 17.

Tentative identifications of many of the modes

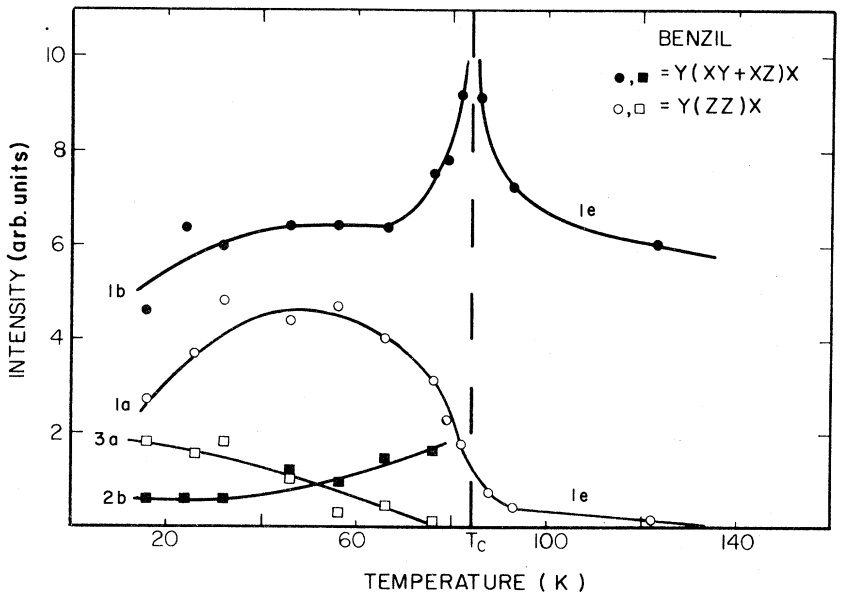

FIG. 12. Temperature dependence of the intensities of the soft modes of benzil above and below T_c (dashed line). Darkened symbols (● and ■) denote B modes below T_c and open symbols (○ and □) denote A modes below T_c.

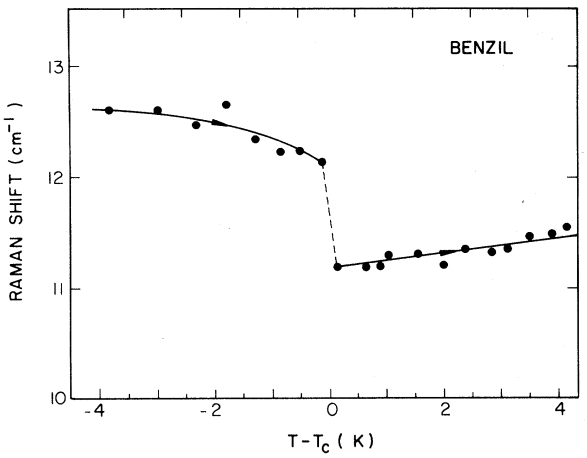

FIG. 13. Temperature dependence of the Raman shift of the B component of the soft E mode in the vicinity of the solid-to-solid phase transition in benzil.

observed in the present study are given in Table VI. The corresponding frequencies are those measured at 16 K. The five B components associated with the five E modes are labeled 1b, 9b, 10b, 13b, and 16b. As seen in Figs. 7 and 9, these components are found to be continuous with the five E modes of the upper phase. Lines 1a and 1b are associated with the soft E mode. On the basis of their frequency and intensity characteristics, the modes labeled 3a and 2b are identified as the A and B components, respectively, of the soft Γ_2 mode. The A modes labeled 6a, 8a, and 13a are associated with the three A_1 modes of the upper phase since no discontinuities in their frequencies or intensities were observed at T_c (see Figs. 8 and 10). The lines 9a and 16a are also seen to merge continuously with the two E modes located at 50.4 and 82.5 cm^{-1} (at T_c), respectively. Since the $2a_1$ and the $2e$ lines located ~ 38 cm^{-1} at room temperature are observed to remain nearly degenerate for all temperatures above 84 K, it is likely that the A component of this E mode is degenerate with that of the A_1 mode for temperatures less than 84 K. Line 8a is thus believed to consist of two A modes that are accidentally degenerate. This conjecture is supported by the Raman activity exhibited by this line in both $X(YZ)Y$ and $X(ZZ)Y$ scattering geometries. Line 11a is believed to be associated with the E mode located at 64.5 cm^{-1} at 84 K since it appears just below T_c and has a comparable frequency. Owing to the effects of the $Y(ZZ)X$ scattering geometry, the intensities of the A components of the E modes are weak near T_c and the above assignments were confirmed by recording similar spectra in a $X(YZ)Y$ scattering geometry.

In our study we have identified the parentage of 15 out of the 36 lines observed in the monoclinic phase. All the Raman-active modes above T_c have counterparts below T_c. According to the predictions summarized in Table IV, the remaining unassigned modes of the monoclinic phase originate from the Raman-inactive Γ_1 ($\vec{k}^*_M$) and Γ_2 ($\vec{k}^*_M$) modes of the trigonal phase.

The preceding discussions have shown that the re-

TABLE VI. Identification of Raman-active external phonon modes below 84 K.

$Y(ZZ)X$: A modes			$Y(XY+XZ)X$: B modes		
Line	Frequency (16 K) (cm^{-1})	Parent mode	Line	Frequency (16 K) (cm^{-1})	Parent mode
1a	13.0	1e (soft)	1b	12.9	1e (soft)
2a	18.6	?	2b	18.4	Γ_2 (soft)
3a	21.6	Γ_2 (soft)	3b	21.5	?
4a	22.6	?	4b	26.0	?
5a	26.2	?	5b	31.2	?
6a	31.5	$1a_1$	6b	35.3	?
7a	38.0	?	7b	38.3	?
8a	44.1	$2a_1+2e$	8b	43.7	?
9a	49.7	3e	9b	49.4	2e
10a	53.5	?	10b	53.1	3e
11a	60.2	4e	11b	58.9	?
12a	68.0	?	12b	63.2	?
13a	75.8	$3a_1$	13b	65.1	4e
14a	78.7	?	14b	68.3	?
15a	82.6	?	15b	74.8	?
16a	90.1	5e	16b	82.8	5e
17a	95.6	?	17b	89.9	?
			18b	92.1	?
			19b	96.3	?

sults of the present Raman scattering study are completely consistent with the predictions of the phenomenological model proposed in Ref. 17. However, as mentioned earlier, benzil is biaxial below T_c and exhibits a multidomain structure. The different orientations of the domains and the optical activity associated with the two optic axes can lead to imperfect polarization results. Some indication of this breakdown was pointed out earlier in the polarized $Y(ZZ)X$ spectra shown in Fig. 8. Upon examination of the frequencies listed in Table VI, it is clear that there is a near coincidence in the frequency shifts of several A and B components. It is possible, if the leakage is significant, that the observed A and B components may not all be independent phonon modes, but rather, are due to fewer modes that are seen in both polarizations. It is difficult to establish unequivocally from the present data which lines, if any, are due to leakage. This difficulty is compounded by the fact that one expects as many as 40 $(17A+23B)$ independent external modes below T_c, each having a typical instrumental halfwidth of ~ 3 cm^{-1}, distributed over the frequency range from 15 to 90 cm^{-1}. As a result, it is possible to have considerable overlapping of the modes. In the most extreme case, if it is assumed that the only additional Raman-active modes observed below T_c are the well-established soft modes, then the total number of independent Raman-active modes would only be 15:

$$3A\ (A_1)+5A\ (E)+5B\ (E)+A\ (\Gamma_2)+B\ (\Gamma_2)\ .$$

(The symbol enclosed in the parenthesis indicates the symmetry of the parent mode above T_c.) Within the resolution limits of the present measurements, the spectra presented earlier in Figs. 7 and 8 allow the identification of a minimum of 22 independent modes at 16 K. Thus it is clear that, even in the worst case, at least seven additional components associated with the Γ_1 and Γ_2 modes of the upper phase arise from the fourfold expansion of the primitive unit cell at the phase transition.

V. CONCLUDING REMARKS

Raman scattering techniques provide an excellent means to study structural phase transitions in solids. The high degree of resolution allows for an accurate determination of the frequency, linewidth, and intensity changes that occur near the transition temperature. The data presented here amply demonstrate this capability and allow the results of the present Raman scattering study of the phase transition in benzil to be compared with the theoretical predictions of the phenomenological model in Ref. 17. The two soft optic modes predicted by this dual order-parameter model were indeed observed: (1) a doubly degenerate E-symmetry mode $(q=0)$ of the trigonal phase which is related to the primary order parameter $\{\eta_i\}$, and (2) a mode of Γ_2 $(\vec{k}^*_M)$ symmetry which is Raman inactive above T_c and is related to the secondary order parameter $\{\zeta_i\}$. The former induces the $D_3^4 \rightarrow C_2^3$ symmetry change while the latter is associated with the fourfold expansion of the primitive unit cell. This expansion of the unit cell gives rise to many new Raman-active modes below T_c which have been observed for the first time in the present study. The Raman spectra below T_c show that the new modes emerge in two stages—the appearance of the two components of the soft mode of Γ_2 $(\vec{k}^*_M)$ symmetry close to T_c is followed by the occurrence of many new lines well below T_c. If the leakage of the forbidden lines in a given polarization configuration can be confidently neglected, then the number and symmetry of the modes observed below T_c are in excellent agreement with those predicted on the basis of Raman activity conferred on them at the phase transition through anharmonic coupling with Raman-active modes.

Attempts to verify the predicted crossing of the A and B components of the soft E mode below T_c were inconclusive. However, detailed measurements of the soft E mode revealed a discontinuous jump of ~ 1 cm^{-1} in its frequency and verifies the first-order nature of the phase transition. Terauchi *et al.*[32] have studied with x rays the temperature dependence of the angles between the optic axis and the twofold axes in the basal plane; the changes in these angles show an unmistakable first-order transition at T_c and give yet another confirmation of the first-order nature of the phase transition. Their results also show clear evidence of the cell enlargement below T_c, the appearance at T_c of the $(\frac{1}{2}\frac{1}{2}6)$ reflection and increase in its intensity with decreasing temperature, and diffuse x-ray scattering around $(\frac{1}{2}\frac{1}{2}6)$ above T_c. All these features constitute further support to the importance of the zone-boundary instability invoked in the phenomenological model.

ACKNOWLEDGMENTS

One of us (A.K.R.) thanks the National Science Foundation for partial support of the work reported in this paper (Grant Nos. DMR-77-27248 and DMR-81-06144). We are indebted to the late Miss Louise Roth, who grew the benzil crystals of exceptional quality. We also thank Professor Swaminatha S. Sundaram and Larry L. Abels for many helpful discussions and for their continued interest in this work.

APPENDIX: THE ONSET OF RAMAN ACTIVITY AT A PHASE TRANSITION

Raman-inactive modes can become Raman active by coupling to normal modes which are already Raman active. Since the inactive mode is also a normal mode of vibration above the transition temperature, it can only couple to the other normal modes via an anharmonic interaction. Consider the case of such a coupling between a Raman-active mode with displacement η and a Raman-inactive mode with displacement ζ. Above the transition temperature the potential energy can be written as

$$U=\tfrac{1}{2}m_1\omega_1^2\eta^2+\tfrac{1}{2}m_2\omega_2^2\zeta^2+\delta\eta\zeta^2 , \tag{A1}$$

where the last term represents the anharmonic coupling between the two modes with a coupling constant δ. Suppose that below the transition temperature T_c both η and ζ take on the spontaneous values η_s and ζ_s, respectively, which minimize the potential energy. The atoms of the crystal will then vibrate about these new equilibrium positions with displacements x and z, and the potential energy below T_c can be written as

$$U(T<T_c)=\tfrac{1}{2}m_1\omega_1^2(\eta_s+x)^2+\tfrac{1}{2}m_2\omega_2^2(\zeta_s+z)^2 +\delta(\eta_s+x)(\zeta_s+z)^2 . \tag{A2}$$

Since $U(\eta_s,\zeta_s)$ is a minimum for $T<T_c$, Eq. (A2) reduces to

$$U(T<T_c)=\tfrac{1}{2}m_1\omega_1^2x^2+\tfrac{1}{2}m_2\omega_2^2z^2+2\delta\zeta_s xz+\cdots . \tag{A3}$$

Hence, to lowest order, the components x and z become linearly coupled and the new normal modes of the crystal for $T<T_c$ are linear combinations of the old ones for $T>T_c$. The new normal modes are found by writing the potential energy as a sum of two squares. By assuming that the coupling is small and that $\frac{1}{2}m_1\omega_1^2>\frac{1}{2}m_2\omega_2^2$, the potential energy below T_c can be written as

$$U(T<T_c)=\tfrac{1}{2}M_1\Omega_1^2X^2+\tfrac{1}{2}M_2\Omega_2^2Z^2+\cdots , \tag{A4}$$

where

$$M_1\Omega_1^2=m_1\omega_1^2+\frac{4\delta^2\zeta_s^2}{m_1\omega_1^2-m_2\omega_2^2} ,$$

$$M_2\Omega_2^2=m_2\omega_2^2-\frac{4\delta^2\zeta_s^2}{m_1\omega_1^2-m_2\omega_2^2} ,$$

and

$$Z=z-\frac{2\delta\zeta_s}{m_1\omega_1^2-m_2\omega_2^2}x .$$

Above the transition temperature, the mode characterized by η is Raman active while the mode associated with ζ is not. Below T_c, the coordinates of the new normal modes are X and Z. For weak coupling, X remains approximately equivalent to x and, hence, is still Raman active. At the same time, Z also has a small Raman-active x component. Consequently, this mode is also Raman active below T_c and its Raman strength is proportional to the square of the coupling constant, i.e., $I\sim\delta^2\zeta_s^2$. Since the spontaneous value of ζ_s vanishes above T_c, the Raman strength of this mode must also vanish at the phase-transition temperature. We note that there are some restrictions on the type of anharmonic coupling terms which give rise to the Raman activity. For example, if the Raman-inactive degree of freedom does not acquire a spontaneous value below T_c, it must appear linearly in the anharmonic term. Such considerations allow the use of symmetry to sort out the anharmonic terms effective in the induced Raman activity.[33]

*Present address: Gould Research Center, Rolling Meadows, Illinois 60008

[1]C. J. Brown and S. Sadanaga, Acta Crystallogr. 18, 158 (1965).
[2]P. H. Esherick and B. E. Kohler, J. Chem. Phys. 59, 6681 (1973).
[3]G. Odou, M. More, and V. Warin, Acta Crystallogr. Sect. A 34, 459 (1978).
[4]R. Claus, H. H. Hacker, H. W. Schrötter, J. Brandmüller, and S. Haussühl, Phys. Rev. 187, 1128 (1969).
[5]S. A. Solin and A. K. Ramdas, Phys. Rev. 174, 1069 (1968).
[6]F. Stenman, J. Chem. Phys. 51, 3141 (1969).
[7]J. Sapriel, A. Boudou, and A. Perigaud, Phys. Rev. B 19, 1484 (1979).
[8]D. R. Moore, V. J. Tekippe, and A. K. Ramdas, Bull. Am. Phys. Soc. 25, 37 (1980).
[9]D. R. Moore, V. J. Tekippe, and A. K. Ramdas, Bull. Am. Phys. Soc. 25, 166 (1980); 27, 324 (1982).
[10]R. Vacher, M. Boissier, and J. Sapriel, Phys. Rev. B 23, 215 (1981).
[11]B. Wyncke, F. Brehat, and A. Hadni, Ferroelectrics 25, 617 (1980).
[12]A. Dworkin and A. H. Fuchs, J. Chem. Phys. 67, 1789 (1977).
[13]See, for example, J. F. Scott, Rev. Mod. Phys. 46, 83 (1974), for a comprehensive review.

[14]Preliminary reports were given in Ref. 8 and D. R. Moore, V. J. Tekippe, and A. K. Ramdas, Bull. Am. Phys. Soc. 26, 486 (1981).

[15]D. R. Moore, V. J. Tekippe, A. K. Ramdas, and J. C. Toledano, J. Phys. (Paris) Colloq. 42, C6-785 (1981).

[16]R. Blinc and B. Žekš, *Soft Modes in Ferroelectrics and Antiferroelectrics* (North-Holland, Amsterdam, 1974).

[17]J. C. Toledano, Phys. Rev. B 20, 1147 (1979).

[18]S. Bhagavantam and T. Venkatarayudu, *Theory of Groups and Its Applications to Physical Problems* (Andhra University Press, Waltair, India, 1962).

[19]L. Couture and J. P. Mathieu, J. Phys. Radium 10, 145 (1949).

[20]We follow the notation in E. B. Wilson, J. C. Decius, and P. C. Cross, *Molecular Vibrations* (McGraw-Hill, New York, 1955).

[21]J. Zak, A. Cacher, H. Gluck, and Y. Gur, *The Irreducible Representations of Space Groups* (Benjamin, New York, 1969).

[22]D. R. Moore, Ph.D. thesis, University of Illinois at Chicago Circle, 1981 (unpublished).

[23]L. D. Landau and E. M. Lifshitz, *Statistical Physics* (Addison-Wesley, Reading, Massachusetts, 1958), p. 443.

[24]P. Toledano and J. C. Toledano, Phys. Rev. B 14, 3097 (1976).

[25]V. E. Naish and V. N. Syromyatnikov, Kristallografiya 21, 1085 (1976) [Sov. Phys.—Crystallogr. 21, 627 (1976)].

[26]P. A. Fleury, in *Phase Transitions—1973,* edited by L. E. Cross (Pergamon, New York, 1973), p. 195.

[27]J. Holakovsky, Phys. Status Solidi B 56, 615 (1973).

[28]Model 8DT Super Vari-Temp optical Dewar, Janis Research Corporation, Inc., 22 Spencer Street, Stoneham, Massachusetts 02180.

[29]Cryogenic Research Company, Inc., 5401 Western Avenue, P. O. Box 881, Boulder, Colorado 80302.

[30]W. G. Cady, *Piezoelectricity* (Dover, New York, 1964).

[31]The scattering geometry is denoted by the notation now common in the literature: By $i(kl)j$, one denotes light incident along i and polarized along k, and scattered along j and analyzed along l. T. C. Damen, S. P. S. Porto, and B. Tell, Phys. Rev. 142, 570 (1966).

[32]H. Terauchi, T. Kojima, K. Sakaue, and F. Tajiri, Ferroelectrics 39, 1155 (1981); J. Chem. Phys. 76, 612 (1982).

[33]J. Petzlet and V. Dvořák, J. Phys. C 9, 1571 (1976); 9, 1587 (1976).